ISSN 0915-633X

# NATIONAL INSTITUTE FOR FUSION SCIENCE

## Drift-kink Instability Induced by Beam Ions in Field-reversed Configurations

K. Nishimura, R. Horiuchi and T. Sato

(Received - Apr. 23, 1999 )

NIFS-595 Apr. 1999



RESEARCH REPORT
NIFS Series

NAGOYA, JAPAN

# Drift-kink instability induced by beam ions in field-reversed configurations

Kazumi Nishimura, Ritoku Horiuchi, and Tetsuya Sato
*Theory and Computer Simulation Center, National Institute for Fusion Science, Toki 509-5292, Japan*

**abstract**

The drift-kink instability in field-reversed configurations with a beam component is investigated by means of a three-dimensional particle simulation. The unstable mode with the toroidal mode number $n = 4$ grows with the rate $\gamma \sim 0.1 - 1.0\omega_{ci}$ for a strong beam current and deforms the plasma profile along the beam orbit in the vicinity of the field-null line. This mode is nonlinearly saturated as a result of the relaxation of current profile. Both the saturation level and the growth rate tend to increase as the ratio of the beam current to the plasma current $I_b/I_p$ increases. It is also found that there is a threshold value of the beam velocity $v_b \sim v_{Ti}$ (ion thermal velocity) for the excitation of the instability.

KEYWORDS: FRC plasmas, drift-kink instability, tilt instability, particle simulation

## 1 Introduction

The compact torus is attractive for a fusion reactor because it has some superior features compared with the representative nominated reactor, e.g., tokamak. Since the diamagnetic toroidal current creates the poloidal magnetic field, it does not need the toroidal coil inherently, then the size of the compact torus reactor tends to be smaller. Furthermore, since there is no structure intersecting plasma torus, it is easy to transfer the plasma along the axial direction for the additional heating or the fuel supply. A field-reversed configuration (FRC) is grouped into the compact tori. Since the pressure of plasmas confined within the separatrix reaches its maximum value in the vicinity of the O-point (the field-null line) and the toroidal magnetic field does not exist ideally, the averaged plasma beta $\langle\beta\rangle$ tends to be high in FRC plasmas ($\langle\beta\rangle \sim 1$).

Tilt instability is known as one of the most dangerous instabilities to disrupt FRC plasmas completely. The analysis based on the ideal magnetohydrodynamic (MHD) theory predicts that FRC plasmas will be unstable against the tilt mode if the shape of its magnetic separatrix is prolate.[1-3] However, many experimental observations show that FRC plasmas remain stable much longer than the tilt growth time.[4-6] Until now, many physical effects which are not taken into account in an ideal MHD theory have been studied in order to explain this contradiction.[7-12] Recent studies[13,14] by means of the three-dimensional particle simulation have revealed that the tilt mode is stabilized for a large plasma beta value at the magnetic separatrix ($\beta_{sp} \geq 0.2$) by the anchoring ions which play a role to hold the unstable internal plasma to the stable external plasma. The value of $\beta_{sp}$ is observed to be around 0.5 in actual experiments.[15] This may give an explanation why the tilt instability has not been observed in many experiments.

In order to apply FRC plasmas for nuclear fusion device, not only stability but also confinement should be improved to be better. The particle confinement is generally improved to be better as the $\beta_{sp}$ decreases, while it becomes impossible to suppress the instability only by decreasing $\beta_{sp}$. Then the other stabilizing method is needed for future devices. Over the last few decades, the beam injection into FRC plasmas is considered to be utilized for suppressing the unstable mode.[16-18] Horiuchi *et al.*[14] carried out the three-dimensional macroscale electromagnetic particle simulation to investigate the ion beam effect in the stability of FRC plasmas and found that the beam injection is effective to keep FRC plasmas stable.

Recently, we have found from the detailed analysis of the simulation data[14] that a low frequency electromagnetic instability grows in the vicinity of the field-null line for a peaked current profile with a localized ion beam and saturates in the early phase of the simulation. This kink-like mode locally deforms the plasma profile on the midplane. The detailed analysis leads us to the conclusion that this mode can be the drift-kink instability (DKI) excited in the FRC plasmas. In a field of space plasma physics, the stability of a current sheet has been an interesting subject in connection with the energy release of substorms. The DKI is a represen-

tative instability of a current sheet and is thought to be one of the candidates of the origin for the onset of substorms. Several theoretical analyses (e.g., kinetic theory[19,20] and two-fluid theory[21,22]) and simulation studies[21,23,24] concerning the DKI in the Harris equilibrium[25] have been made. According to these analyses, the DKI is triggered in the enough thin current sheet and the low frequency electromagnetic mode is excited at the center of the neutral sheet. The drift motion of ions along the current sheet is important for the development of the DKI. It has been shown that the growth rate of the DKI tends to decrease as the ratio $\rho_{i0}/L$ decreases, where $\rho_{i0}$ is the typical ion gyroradius and $L$ is the sheet thickness. The critical thickness has been estimated to be $\rho_{i0}/L \sim 1$.[26] The plasma profile on the midplane of the FRC plasmas considered in our simulation model is very similar to the Harris equilibrium. That is, the strong antiparallel magnetic field exists at the both sides of the peaked beam current, the width of which is comparable to the typical ion Larmor radius.

The purpose of this paper is to examine the properties of this new instability appeared in FRC plasmas with a beam component. The outline of this paper is as follows. We describe in detail our simulation model and method in Sec. 2. Simulation results are discussed in Sec. 3. Summary and discussion are given in Sec. 4.

## 2 Simulation Model

We consider FRC plasmas confined by a uniform external magnetic field $B_N$ within the cylindrical conducting vessel. The height of this vessel $Z_D$ is fixed to 6 times the vessel radius $R_D$ in this paper. The time development of all particles (thermal ion, thermal electron, and beam ion) and field quantities are solved with using the three-dimensional electromagnetic particle simulation code.[8] It is assumed that the physical quantities are periodic at the boundary of $z$ axis and the vessel wall is a rigid perfect conductor. The particles are elastically reflected at the vessel wall. The equations to be solved are the equations of motion

$$\frac{d(\gamma_j \boldsymbol{v}_j)}{dt} = \frac{q_j}{m_j}\left(\boldsymbol{E} + \frac{\boldsymbol{v}_j}{c}\times\boldsymbol{B}\right), \quad (1)$$

$$\frac{d\boldsymbol{x}_j}{dt} = \boldsymbol{v}_j, \quad (2)$$

and the Maxwell equations

$$\frac{1}{c}\frac{\partial \boldsymbol{B}}{\partial t} = -\nabla\times\boldsymbol{E}, \quad (3)$$

$$\frac{1}{c}\frac{\partial \boldsymbol{E}}{\partial t} = \nabla\times\boldsymbol{B} - \frac{4\pi}{c}\boldsymbol{j}, \quad (4)$$

$$\nabla\cdot\boldsymbol{E} = 4\pi\rho, \quad (5)$$

$$\nabla\cdot\boldsymbol{B} = 0, \quad (6)$$

where $\boldsymbol{x}_j(t), \boldsymbol{v}_j(t)$, $m_j$ and $q_j$ are the position, the velocity, the rest mass and the charge of the $j$th particle, and the relativistic $\gamma$-factor of the $j$th particle is defined by

$$\gamma_j = 1/\sqrt{1-(\boldsymbol{v}_j\cdot\boldsymbol{v}_j)/c^2}. \quad (7)$$

The current density $\boldsymbol{j}(\boldsymbol{x},t)$ is obtained by summing over all the particles, namely,

$$\boldsymbol{j}(\boldsymbol{x},t) = \sum_{j=1}^{N_{tot}} q_j \boldsymbol{v}_j(t)\ S[\boldsymbol{x}-\boldsymbol{x}_j(t)], \quad (8)$$

where $N_{tot}$ is the total number of particles and $S(\boldsymbol{x})$ is the form function of particles.[27,28]

Particle pusher and gather processes are carried out in the rectangular coordinates $(x,y,z)$ where the simulation domain is implemented on a $(49\times 49\times 32)$ point grid and its volume is given by $(2R_D\times 2R_D\times 2Z_D)$. On the other hand, the electromagnetic field is solved in the cylindrical coordinates $(r,\theta,z)$ so that the boundary condition on the conducting wall can be satisfied with a high precision. The cylindrical vessel is embedded inside the rectangular simulation box so as to contact its surface with four sides of the rectangular box. The $(33\times 32\times 32)$ space grids are used in this calculation. We have examined the numerical stability and accuracy of this scheme by changing the simulation parameters such as the number of space grids, number of particles, and so on, and have chosen their values. It is found that one of the most effective methods to reduce a numerical noise and obtain physically reliable results is to increase the number of particles in a cell. The total number of thermal particles is fixed to $10^6$ in the present simulation.

Two-dimensional MHD equilibrium solution is used for an initial profile of the simulation. In the case where the beam ions exists, we adopt the MHD equilibrium including a beam component,

$$-\nabla P + \frac{1}{c}\boldsymbol{j}_d\times\boldsymbol{B} = 0, \quad (9)$$

$$\nabla\times\boldsymbol{B} = \frac{4\pi}{c}(\boldsymbol{j}_d+\boldsymbol{j}_b), \quad (10)$$

with the Cobb's pressure model[10], which can control both the current profile and the beta value at the separatrix easily,

$$P(\Psi) = \begin{cases} P_0(K_0 - \chi - \frac{1}{2}D\chi^2) & \text{for } \chi \le 0 \\ P_0 K_0 e^{-\chi/K_0} & \text{for } \chi > 0, \end{cases} \quad (11)$$

where $j_d$ is the diamagnetic current density, $j_b$ is the beam current density, $P(= P_i + P_e)$ is the total pressure, $\chi = \Psi/|\Psi_{ax}|$, $\Psi_{ax}$ is the value of $\Psi$ at the field-null ($\chi = -1$), and $P_0$ is constant. The parameter $K_0$ is represented by two important parameters, $\beta_{sp}$ and $D$ as $K_0 = \beta_{sp}(1 - D/2)/(1 - \beta_{sp})$. The parameter $\beta_{sp}$ is the normalized pressure value at the magnetic separatrix on the midplane and also represents roughly the plasma beta value at the separatrix, $D$ is the hollowness parameter which controls the current distribution. That is to say, the current profile of the equilibrium state, $j_\theta/r$, becomes peaked for $D < 0$, flat for $D = 0$, and hollow for $D > 0$. If the beam current density is determined, the set of these equations can be solved numerically under the assumption that the number density of beam ions is much smaller than that of thermal ions. The spatial distribution of beam current is assumed to be in a Gaussian form, of which the standard deviation is given by $0.23(r_{sp} - R)$ for the radial direction, where $r_{sp}$ and $R$ is the separatrix radius and the radius of the field-null on the midplane, respectively, and $0.23(r_{sp} - R) \times E$ for the $z$-direction, where $E$ is the separatrix elongation. For an initial condition, we assume that the beam ions are injected along the azimuthal direction with the toroidal velocity $v_b$ and the temperature $T_b = 0$. The velocity $v_b$ and the center position $r_b$ of beam distribution are determined so as to satisfy the force balance equation. Figure 1 shows (a) the contour plots of thermal ion density and (b) that of beam ion density in the poloidal cross section in the initial equilibrium state. The outer curved line represents the magnetic separatrix in each figure. As the figure indicates, the density distribution of beam ions is concentrated in the vicinity of the field-null line on the midplane.

In this calculation, all the physical variables are normalized by the following four fundamental quantities : $c$ (speed of light), $q_N$ (elementary charge), $m_N$ (electron mass), and $\omega_N$ (electron cyclotron frequency defined as $q_N B_N/m_N c$). The number of beam ions can be changed freely as one of the controlled parameters in this simulation. It is also assumed that the beam ions are the same kind of thermal ions, i.e., $q_b = q_i$, where $q_b$ is the charge of the beam ion and $q_i$ is that of the thermal ion.

The profile control parameters are fixed to $\beta_{sp} = 0.02$ and $D = -0.6$ for all cases. The particle confinement should be improved to be better in order to apply FRC plasmas for nuclear fusion device, as we have mentioned in Sec. 1. For that reason, the low value of $\beta_{sp}$ is desirable. On the other hand, it has been shown that the profile specified by these values ($\beta_{sp} = 0.02, D = -0.6$) becomes unstable against the tilt instability if a beam component does not exist.[13] Our original aim of injecting ion beams into FRC plasmas is to examine the ion beam effect on the tilt instability. Thus, we have chosen these values as a typical example of the unstable profile for the tilt mode and carried out simulation runs.

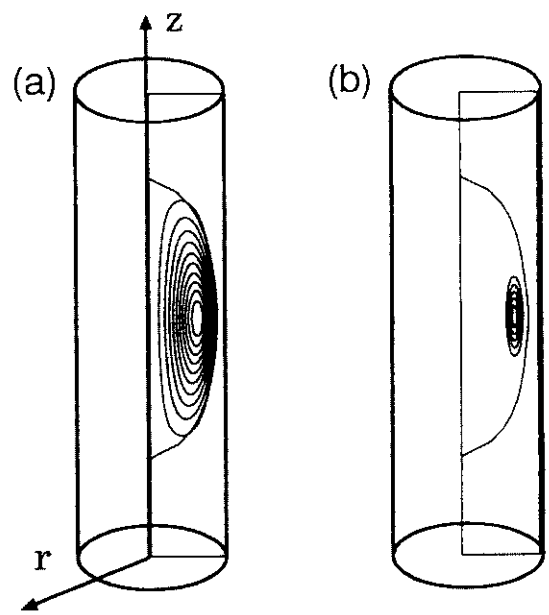


Fig. 1. Contour plots of (a) the thermal ion density and (b) the beam ion density in the poloidal cross section at the initial period. The columns represent the conducting vessel and the magnetic separatrix is also depicted in each figure.

## 3 Simulation Result

The typical parameters are as follows : the mass ratio is $m_i/m_e = 50$, the ion cyclotron frequency defined by the vacuum magnetic field $B_N$ is $\omega_{ci} = 0.02\omega_N$, the ion thermal velocity is $v_{Ti} = 0.015c$, the ratio of thermal ion temperature to thermal electron temperature is $T_i/T_e = 1$, the radius of the cylindrical vessel is $R_D = 5.63c/\omega_N$ ($= 7.5v_{Ti}/\omega_{ci}$), and the toroidal current of thermal plasma is $I_p = 8.9q_N\omega_N$. The Alfvén transit time $t_A$ ($= R_D/v_A$ where $v_A$ is the Alfvén velocity defined by the ion density at the field-null line and the magnetic field at the wall on the midplane) is nearly equal to $200\omega_N^{-1}$. The other important parameters used for the simulation are listed in Table I.

Figure 2 shows the radial distributions of the current density on the midplane at three different time periods for the case RA5. The typical profile of the current density with a beam component

has a sharp peak in the vicinity of the field-null line at the initial stage. The sharpness of the initial current distribution generally tends to be large as the current ratio $I_b/I_p$ increases. One can see in Fig. 2 that the peaked current profile relaxes to the smoothed profile as time elapses. This relaxation is followed by both the decrement of the beam velocity $v_b$ and the spread of the distribution of beam ions in the radial direction.

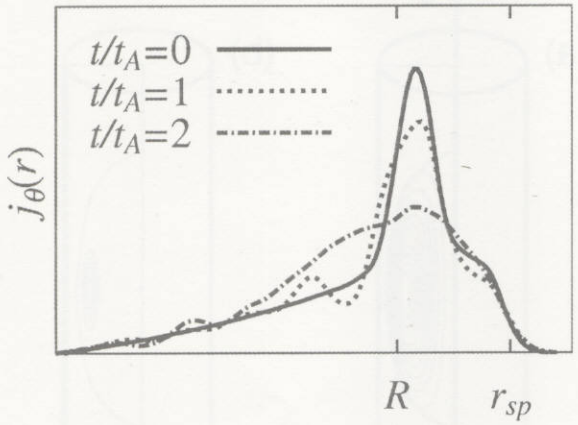


Fig. 2. Radial profile of the averaged toroidal current density on the midplane at three different time periods for the case RA5, where $r_{sp}$ and $R$ is the separatrix radius and the radius of the field-null on the midplane, respectively.

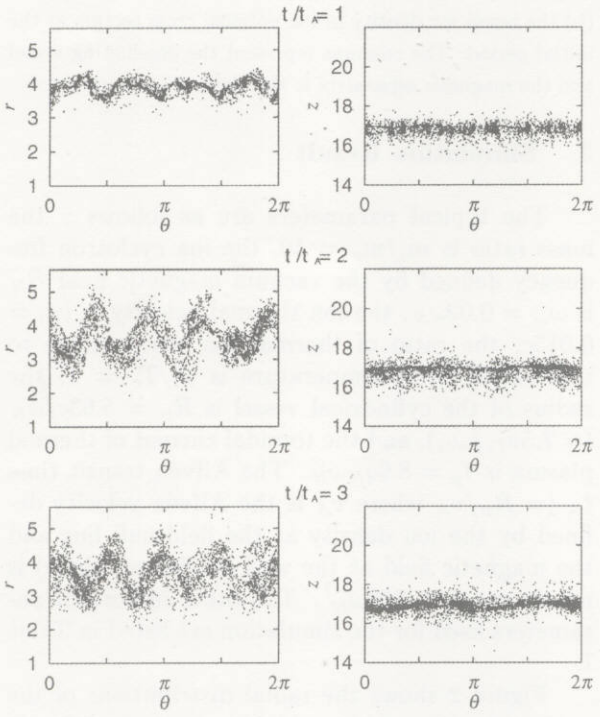


Fig. 3. Time sequential plots of beam ions projected on (left) the $\theta - r$ space and (right) the $\theta - z$ space for the same case as Fig. 2.

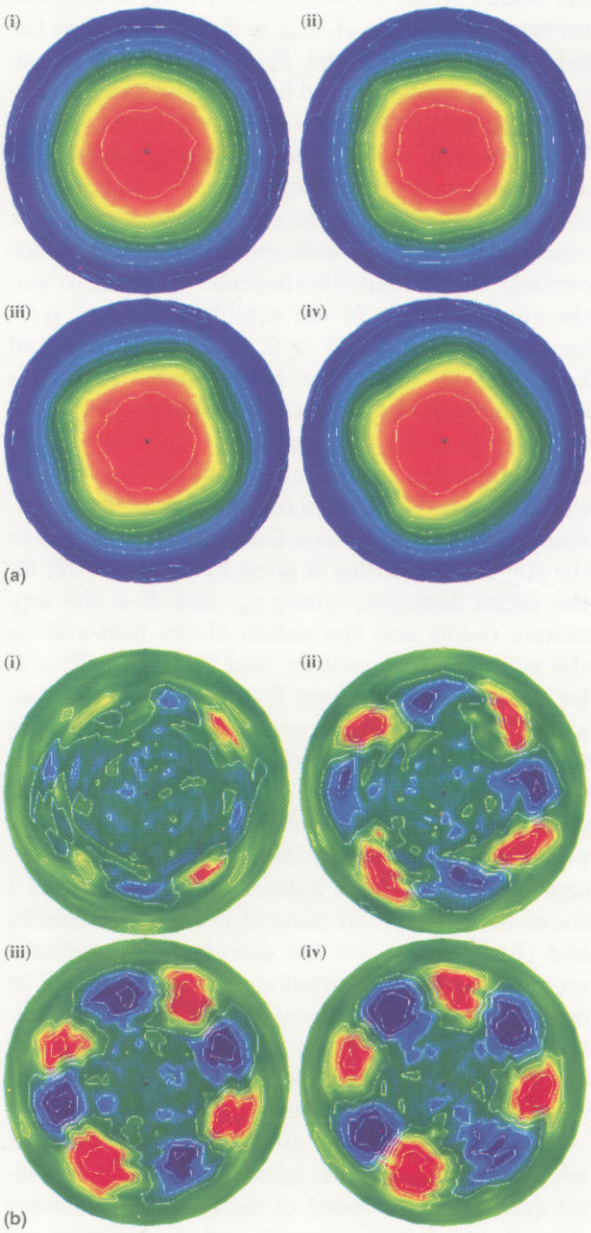


Fig. 4. Time sequential color-coded plots of (a) the magnetic field $B_z$ contours and (b) the perturbed magnetic field $\Delta B_z$ contours on the midplane for the same case as Fig. 2. (i) $t/t_A = 1.0$, (ii) 1.5, (iii) 2.0, (iv) 2.5.

In order to make clear the behavior of beam ions, we plot the distribution of all beam ions in Fig. 3 for the same case as Fig. 2. The left and right panels show the time evolution of the distribution of beam ions in the $\theta - r$ space and that in the $\theta - z$ space, respectively. The wavy structure is generated in the $\theta - r$ space as time elapses, thus the beam ion distribution changes dramatically from the initial distribution. On the other

hand, the ion distribution in the $\theta - z$ space hardly changes. Since the magnetic field is dominated by the $z$-component on the midplane, the deviation of the beam profile develops in the perpendicular direction of the magnetic field.

Figure 4 shows (a) the time development of the color-coded contour plots of the $z$-component of the magnetic field $B_z$ and (b) that of the perturbed magnetic field $\Delta B_z$ on the midplane, where $\Delta B_z$ is defined by $B_z(t) - \langle B_z(t) \rangle$ (the bracket stands for the average in the toroidal direction). The strong deformation of the magnetic profile occurs in the vicinity of the field-null line, where the current density with a beam component steepens. It is also found that the mode pattern slowly rotates in the toroidal direction with the real frequency $\omega_r = 0.13\omega_{ci}$ for this case. This value is much smaller than the rotation frequency $\Omega$ ($= v_b/r_b \sim 1.10\omega_{ci}$), the drift frequency $\omega_*$ ($= k_\theta v_b \sim 4.4\omega_{ci}$), and the betatron frequency in the radial direction $\omega_{br}$ ($\sim 1.47\omega_{ci}$). This mode propagates in the same direction as the beam circular motion. Judging from the mode pattern of the perturbed magnetic field, it seems reasonable to suppose that this unstable mode corresponds to the DKI driven by the peaked current. The real frequency of our simulation results, however, is a little smaller than that obtained from the previous analyses,[19-24] which is roughly within the range from $0.1\omega_{ci}$ to $\omega_{ci}$. The difference may be explained in terms of both the geometry and the equilibrium profile.

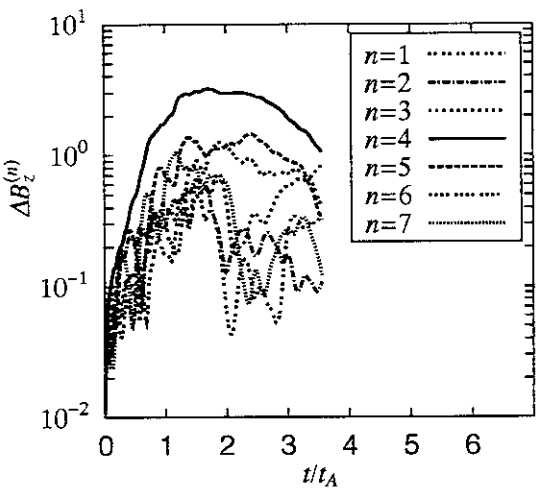


Fig. 5. Time history of the mode amplitude $\Delta B_z^{(n)}$ for different values of toroidal mode number $n$ for the same case as Fig. 2.

The time histories of the amplitude $\Delta B_z^{(n)}$ of each toroidal mode ($n = 1 \sim 7$) are shown in Fig. 5, where the magnetic field is measured at the initial position of the beam ion $r_b$ on the midplane. The $n = 4$ mode grows dominantly and its amplitude is saturated in the early phase of the simulation ($t/t_A \approx 2$). This period corresponds to the time when the initial peaked current profile with the half-width $L \ll \rho_{i0}$ relaxes to the smoothed profile of $L \geq \rho_{i0}$ (see Fig. 2). This suggests the instability is nonlinearly saturated as a result of the relaxation of the current profile. In other words, the ion beam which is localized in an unmagnetized narrow region ($L \ll \rho_{i0}$) spreads over the magnetized wide region ($L \geq \rho_{i0}$) as a result of the nonlinear evolution of the DKI. Thus, the ion magnetization effect may stabilize the DKI for $L \geq \rho_{i0}$. The growth rate of this mode can be estimated to $1.14\omega_{ci}$ from Fig. 5. The toroidal mode number $n$ of the most unstable mode is found to be 4 for all cases in our simulation. Both the real frequency $\omega_r$ and the growth rate $\gamma$ of the $n = 4$ mode are summarized in Table I.

In Fig. 6 (a), the maximum saturation amplitude of the perturbed magnetic field is shown as a function of the beam velocity $v_b/v_{Ti}$ for the cases of $N_b/N_i = 0.01$ and $N_b/N_i = 0.02$. Although the maximum amplitude increases with the beam velocity $v_b/v_{Ti}$ for both cases, one can see that the amplitudes for $N_b/N_i = 0.02$ become larger than that for $N_b/N_i = 0.01$ in the case of the same beam velocity. It is interesting to notice that the growth rate is negligibly small for $v_b < v_{Ti}$ and it starts to increase with $v_b$ as soon as $v_b$ becomes larger than $v_{Ti}$, regardless of the value of $N_b/N_i$. This phenomena can be explained in the followings. We have a rough relation $v_d/v_{Ti} \sim \rho_{i0}/L$ for an MHD equilibrium, where $v_d$ is the average drift velocity, $\rho_{i0}$ is the typical ion Larmor radius and $L$ is the scale length of an equilibrium profile. For a weak beam ($v_b < v_{Ti}$), the scale length $L$ is given by $r_{sp} - R\ (> \rho_{i0})$. i.e., $v_d/v_{Ti} \sim \rho_{i0}/L < 1$. The DKI is stable for $\rho_{i0}/L < 1$.[26] Because the beam is injected in a narrow region ($L \sim (r_{sp} - R)/5 < \rho_{i0}$), the scale length decreases with the beam velocity or the beam current. We have the relations as $v_d/v_{Ti} \sim v_b/v_{Ti} \sim \rho_{i0}/L > 1$ for a strong beam ($v_b > v_{Ti}$). Thus, the strong beam of $v_b/v_{Ti} \gg 1$ destabilizes the DKI because $\rho_{i0}/L \gg 1$. In Fig. 6 (b), the maximum amplitude of the perturbed magnetic field are shown as a function of the number ratio $N_b/N_i$ for the cases of $v_b/v_{Ti} = 2.00$ and $v_b/v_{Ti} = 4.00$. The maximum amplitudes hardly increase with the number ratio for $v_b/v_{Ti} = 2.00$. On the other hand, the amplitudes dramatically increase with the number ratio for $v_b/v_{Ti} = 4.00$.

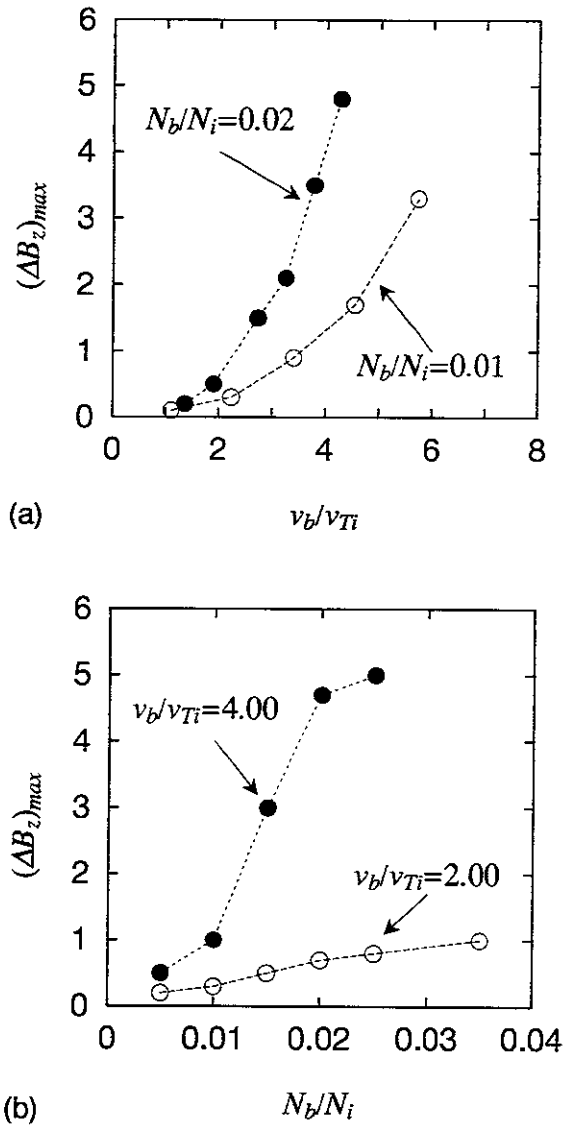


Fig. 6. Dependence of the saturation levels of the $n = 4$ DKI on (a) the beam velocity $v_b/v_{Ti}$ for two different values of $N_b/N_i$ : $N_b/N_i = 0.01$ (open circles) and $N_b/N_i = 0.02$ (closed circles), and (b) the number ratio $N_b/N_i$ for two different values of $v_b/v_{Ti}$ : $v_b/v_{Ti} = 2.00$ (open circles) and $v_b/v_{Ti} = 4.00$ (closed circles).

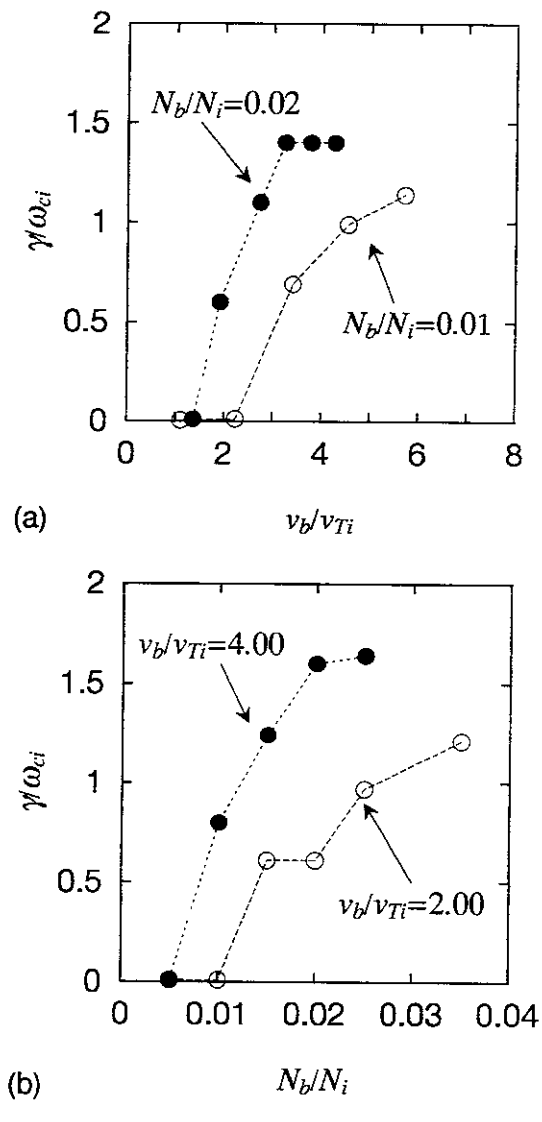


Fig. 7. Dependence of the growth rates of the $n = 4$ DKI on (a) the beam velocity $v_b/v_{Ti}$ for two different values of $N_b/N_i$ : $N_b/N_i = 0.01$ (open circles) and $N_b/N_i = 0.02$ (closed circles), and (b) the number ratio $N_b/N_i$ for two different values of $v_b/v_{Ti}$ : $v_b/v_{Ti} = 2.00$ (open circles) and $v_b/v_{Ti} = 4.00$ (closed circles).

Figure 7 shows the dependences of the growth rate of the $n = 4$ drift-kink mode on $v_b/v_{Ti}$ and $N_b/N_i$ for the same cases as Fig. 6. The growth rate is evaluated by the time development of the perturbed magnetic field, as we have seen in Fig. 5. It is clear that the growth rate $\gamma$ tends to increase as either the beam velocity $v_b/v_{Ti}$ or the number ratio $N_b/N_i$ becomes larger. On the other hand, Fig. 7 indicates that there exists the lower limit of the beam current to excite the DKI.

From these results it is concluded that the new instability excited in the vicinity of the field-null is the drift-kink instability driven by the peaked beam current.

## 4 Summary and Discussion

We have investigated the new electromagnetic instability excited in the vicinity of the field-null line of FRC plasmas by means of a three-dimensional electromagnetic particle simulation. The detailed

analysis leads to the conclusion that this instability corresponds to the drift-kink instability (DKI) driven by the peaked beam current. The important results are summarized in the followings :

(i) In FRC plasmas with a beam component, the DKI is locally generated along the orbit of beam ions in the vicinity of the field-null line and saturates in the early phase ($0 < t/t_A < 2$). The deviation of the profile mainly develops in the perpendicular direction of the magnetic field $B_z$ on the midplane.

(ii) The toroidal mode number of the most unstable drift-kink mode is $n = 4$ in our simulation. The real frequency $\omega_r$ of this mode is observed within the range from $0.02\omega_{ci}$ to $0.15\omega_{ci}$.

(iii) The saturation level of the amplitude and the growth rate $\gamma$ of the drift-kink mode tend to increase as the number ratio $N_b/N_i$ or the velocity of beam ions $v_b/v_{Ti}$ increases.

The first result, (i), means that the DKI grows faster than the tilt instability. The tilt mode has been observed to grow prominently during $2 < t/t_A < 4$ for the no beam cases.[13] The DKI which deforms the local structure of an equilibrium current density may have an influence on the global tilt instability. The correlation between the growth of the DKI and the tilt suppression is an important issue in the future research.

We comment on the rapid growth and the saturation of the DKI. In case of the particle simulation, the initial profile consisting of particles does not exactly coincide with the MHD equilibrium profile because the Larmor radii of particles are finite. Therefore, the initial profile relaxes into the particle equilibrium profile in one ion gyration period ($2\pi/\omega_{ci} \sim 0.4t_A$). On the other hand, the DKI takes a longer time ($t/t_A \sim 2.0 - 3.5$) reaching to the saturation level. Thus, it is always possible to distinguish the initial relaxation phase from the growing phase of the DKI.

The second result, (ii), suggests that the real frequency of our simulation results is a little smaller than that obtained from the previous analyses concerning the DKI in the Harris equilibrium, as we described in Sec. 3. However, one may expect that the difference concerning the real frequency is caused by the difference of the profile between FRC plasmas and the Harris equilibrium.

Let us consider why the $n = 4$ mode is dominant in all simulation runs. According to the linear analysis,[22] the maximum growth rate depends on the parameter $k_z L_b \simeq nL_b/R$, i.e., the half-width of the beam profile $L_b$. For all cases discussed above the half-width $L_b$ is approximately given by $(r_{sp} - R)/5$. In order to confirm this point, we carry out another simulation run with a different value of $L_b$. Shown in Fig. 8 is the temporal evolution of the mode amplitudes for $L_b = 0.099R_D$. It is clearly seen in Fig. 8 that the dominant mode is not $n = 4$ but $n = 5$, and the FRC plasma relaxes into a nonlinear saturation state in a relatively long time ($t \sim 3.5t_A$). This problem should be discussed in detail elsewhere.

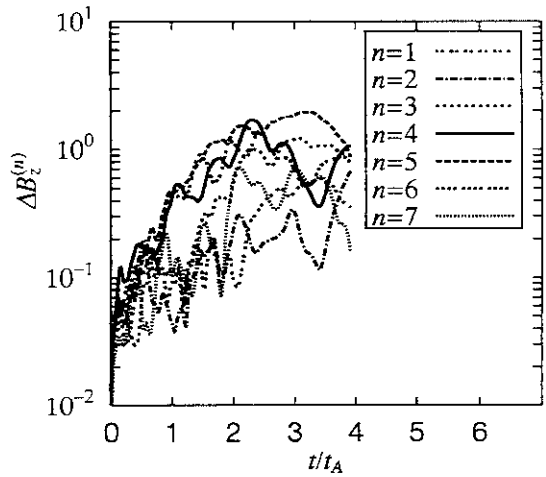


Fig. 8. Time history of the mode amplitude $\Delta B_z^{(n)}$ for different values of toroidal mode number $n$ for the case $N_b/N_i = 0.01, v_b/v_{Ti} = 5.77$, and the half-width of the beam profile $L_b = 0.099R_D$.

## Acknowledgments

One of the authors (K.N.) would like to express his gratitude to Dr. Y. Todo for helpful discussions. The simulation work was performed by employing the Advanced Computing System for Complexity Simulation at the National Institute for Fusion Science (NIFS).

## References

[1] M. N. Rosenbluth and M. N. Bussac, Nucl. Fusion **19**, 489 (1979).
[2] J. H. Hammer, Nucl. Fusion **28**, 488 (1981).
[3] R. A. Clemente and J. L. Milovich, Physics Letters **85A**, 148 (1981).
[4] M. Tuszewski, Nucl. Fusion **28**, 2033 (1988)
[5] J. T. Slough and A. L. Hoffman, Nucl. Fusion **28**, 1121 (1988).
[6] J. T. Slough, A. L. Hoffman, R. D. Milroy, R. Maqueda, and L. C. Steinhauer, Phys. Plasmas **2**, 2286 (1995).
[7] D. C. Barnes, J. L. Schwarzmeier, R. Lewis, and C. E. Seyler, Phys. Fluids **29**, 2616 (1986).
[8] R. Horiuchi and T. Sato, Phys. Fluids **B 2**, 2652 (1990)
[9] L. C. Steinhauer and A. Ishida, Phys. Fluids **B 4**, 645 (1992).

[10]J. W. Cobb, T. Tajima, and D. C. Barnes, Phys. Fluids **B 5**, 3227 (1993).
[11]R. Kanno, A. Ishida, and L. C. Steinhauer, J. Phys. Soc. Jpn. **64**, 463 (1995).
[12]H. Ji, M. Yamada, R. Kulsrud, N. Pomphrey, and H. Himura, Phys. Plasmas **5**, 3685 (1998).
[13]K. Nishimura, R. Horiuchi, and T. Sato, Phys. Plasmas **4**, 4035 (1997).
[14]R. Horiuchi, K. Nishimura, T.-H. Watanabe, and T. Sato, "Kinetic stabilization of tilt disruption in field-reversed configurations," to appear in Nucl. Fusion.
[15]M. Tuszewski, Plasma Phys. Contr. Fusion **26**, 991 (1984).
[16]J. M. Finn and R N. Sudan, Nucl. Fusion **22**, 1443 (1982).
[17]Y. Nomura, J. Phys. Soc. Jpn. **54**, 1369 (1985).
[18]D. C. Barnes and R. D. Milroy, Phys. Fluids B **3**, 2609 (1991).
[19]P. H. Yoon, A. T. Y. Lui, and H. K. Wong, J. Geophys. Res. **103**, 11,875 (1998).
[20]G. Lapenta and J. U. Brackbill, J. Geophys. Res. **102**, 27,099 (1997)
[21]P. L. Pritchett, F. V. Coroniti, and V. K. Decyk, J. Geophys. Res. **101**, 27,413 (1996).
[22]W. Daughton, J. Geophys. Res. **103**, 29,429 (1998)
[23]M. Ozaki, T. Sato, R. Horiuchi, and the Complexity Simulation Group, Phys. Plasmas **3**, 2265 (1996).
[24]Z. Zhu and R. M. Winglee, J. Geophys. Res. **101**, 4885 (1996).
[25]E. G. Harris, Nuovo Cimento **23**, 115 (1962).
[26]K. Yamanaka, Phys. Scr. **17**, 15 (1978).
[27]C. K. Birdsall and A. B Langdon, *Plasma Physics Via Computer Simulation* (McGraw-Hill, New York, 1985) p.168.
[28]R. Horiuchi and T. Sato, Phys. Plasmas **1**, 3587 (1994).

Table I. Simulation results, including number ratio $N_b/N_i$; current ratio $I_b/I_p$; beam velocity $v_b/v_{Ti}$; ratio of field-null to vessel radius $R/R_D$; ratio of separatrix to vessel radius $r_{sp}/R_D$; separatrix elongation $E$; ratio of plasma radius to gyroradius of thermal ions $S_p$; ratio of plasma radius to gyroradius of beam ions $S_b$; real frequency of $n = 4$ mode $\omega_r/\omega_{ci}$; growth rate of $n = 4$ mode $\gamma/\omega_{ci}$.

| RUN | $N_b/N_i$ | $I_b/I_p$ | $v_b/v_{Ti}$ | $R/R_D$ | $r_{sp}/R_D$ | $E$ | $S_p$ | $S_b$ | $\omega_r/\omega_{ci}$ | $\gamma/\omega_{ci}$ |
|---|---|---|---|---|---|---|---|---|---|---|
| R00 | 0.000 | 0.000 | 0.00 | 0.61 | 0.84 | 2.14 | 3.00 | – | – | – |
| RA1 | 0.010 | 0.010 | 1.11 | 0.60 | 0.85 | 2.13 | 4.60 | 4.15 | 0.05 | 0.005 |
| RA2 | 0.010 | 0.020 | 2.24 | 0.61 | 0.85 | 2.13 | 4.72 | 2.11 | 0.15 | 0.01 |
| RA3 | 0.010 | 0.030 | 3.41 | 0.66 | 0.86 | 2.13 | 5.05 | 1.48 | 0.12 | 0.69 |
| RA4 | 0.010 | 0.040 | 4.55 | 0.64 | 0.87 | 2.12 | 4.96 | 1.09 | 0.10 | 0.99 |
| RA5 | 0.010 | 0.050 | 5.72 | 0.66 | 0.88 | 2.11 | 5.08 | 0.89 | 0.13 | 1.14 |
| RB1 | 0.020 | 0.025 | 1.37 | 0.61 | 0.86 | 2.13 | 4.72 | 3.45 | 0.02 | 0.01 |
| RB2 | 0.020 | 0.035 | 1.91 | 0.63 | 0.86 | 2.13 | 4.88 | 2.55 | 0.10 | 0.60 |
| RB3 | 0.020 | 0.050 | 2.73 | 0.65 | 0.87 | 2.13 | 5.08 | 1.86 | 0.10 | 1.10 |
| RB4 | 0.020 | 0.060 | 3.25 | 0.64 | 0.88 | 2.13 | 4.96 | 1.53 | 0.10 | 1.40 |
| RB5 | 0.020 | 0.070 | 3.78 | 0.66 | 0.88 | 2.14 | 5.24 | 1.38 | 0.10 | 1.40 |
| RB6 | 0.020 | 0.080 | 4.27 | 0.66 | 0.89 | 2.14 | 5.08 | 1.19 | 0.10 | 1.40 |
| RC1 | 0.005 | 0.009 | 2.00 | 0.62 | 0.85 | 2.13 | 4.78 | 2.39 | 0.07 | 0.01 |
| RC2 | 0.010 | 0.018 | 2.00 | 0.62 | 0.85 | 2.13 | 4.73 | 2.37 | 0.05 | 0.01 |
| RC3 | 0.015 | 0.027 | 2.00 | 0.64 | 0.86 | 2.13 | 4.91 | 2.46 | 0.12 | 0.61 |
| RC4 | 0.020 | 0.037 | 2.00 | 0.63 | 0.87 | 2.13 | 4.85 | 2.42 | 0.07 | 0.61 |
| RC5 | 0.025 | 0.046 | 2.00 | 0.63 | 0.87 | 2.14 | 4.84 | 2.42 | 0.07 | 0.97 |
| RC6 | 0.035 | 0.067 | 2.00 | 0.65 | 0.88 | 2.14 | 4.98 | 2.48 | 0.07 | 1.21 |
| RD1 | 0.005 | 0.017 | 4.00 | 0.64 | 0.85 | 2.13 | 4.92 | 1.23 | 0.07 | 0.01 |
| RD2 | 0.010 | 0.035 | 4.00 | 0.65 | 0.87 | 2.13 | 4.97 | 1.24 | 0.12 | 0.80 |
| RD3 | 0.015 | 0.054 | 4.00 | 0.64 | 0.88 | 2.12 | 4.96 | 1.24 | 0.10 | 1.24 |
| RD4 | 0.020 | 0.075 | 4.00 | 0.66 | 0.89 | 2.14 | 5.08 | 1.27 | 0.10 | 1.60 |
| RD5 | 0.025 | 0.095 | 4.00 | 0.68 | 0.90 | 2.15 | 5.20 | 1.30 | 0.10 | 1.64 |

## Recent Issues of NIFS Series

NIFS-531 J Uramoto,
*Confirmation Method for Metal Plate Penetration of Low Energy Negative Pionlike or Muonlike Particle Beam under Positive Ions*, Dec 1997

NIFS-532 J Uramoto,
*Pair Creations of Negative and Positive Pionlike (Muonlike) Particle or K Mesonlike (Muonlike) Particle in H2 or D2 Gas Discharge in Magnetic Field*, Dec 1997

NIFS-533 S Kawata, C Boonmee, T Teramoto, L Drska, J Limpouch, R Liska, M Sinor,
*Computer-Assisted Particle-in-Cell Code Development*; Dec 1997

NIFS-534 Y Matsukawa, T Suda, S. Ohnuki and C Namba,
*Microstructure and Mechanical Property of Neutron Irradiated TiNi Shape Memory Alloy*, Jan 1998

NIFS-535 A. Fujisawa, H Iguchi, H Idei, S Kubo, K Matsuoka, S. Okamura, K. Tanaka, T Minami, S. Ohdachi, S. Morita, H Zushi, S Lee, M. Osakabe, R Akiyama, Y Yoshimura, K. Toi, H Sanuki, K. Itoh, A. Shimizu, S Takagi, A Ejiri, C Takahashi, M Kojima, S Hidekuma, K. Ida, S. Nishimura, N Inoue, R. Sakamoto, S -I Itoh, Y. Hamada, M Fujiwara,
*Discovery of Electric Pulsation in a Toroidal Helical Plasma*; Jan 1998

NIFS-536 Lj.R Hadzievski, M.M Skoric, M. Kono and T. Sato,
*Simulation of Weak and Strong Langmuir Collapse Regimes*, Jan. 1998

NIFS-537 H Sugama, W. Horton,
*Nonlinear Electromagnetic Gyrokinetic Equation for Plasmas with Large Mean Flows*, Feb. 1998

NIFS-538 H. Iguchi, T P Crowley, A Fujisawa, S Lee, K Tanaka, T Minami, S. Nishimura, K. Ida, R. Akiyama, Y Hamada, H , Idei M Isobe, M. Kojima, S. Kubo, S. Morita, S. Ohdachi, S Okamura, M Osakabe, K. Matsuoka, C Takahashi and K. Toi,
*Space Potential Fluctuations during MHD Activities in the Compact Helical System (CHS)*; Feb. 1998

NIFS-539 Takashi Yabe and Yan Zhang,
*Effect of Ambient Gas on Three-Dimensional Breakup in Coronet Formation Process*; Feb 1998

NIFS-540 H. Nakamura, K. Ikeda and S Yamaguchi,
*Transport Coefficients of InSb in a Strong Magnetic Field*; Feb. 1998

NIFS-541 J. Uramoto,
*Development of $\nu_\mu$ Beam Detector and Large Area $\nu_\mu$ Beam Source by $H_2$ Gas Discharge (I)*, Mar 1998

NIFS-542 J. Uramoto,
*Development of $bar{\nu}_\mu$ Beam Detector and Large Area $bar{\nu}_\mu$ Beam Source by $H_2$ Gas Discharge (II)*, Mar. 1998

NIFS-543 J. Uramoto,
*Some Problems inside a Mass Analyzer for Pions Extracted from a $H_2$ Gas Discharge*; Mar 1998

NIFS-544 J. Uramoto,
*Simplified $\nu_\mu$ $bar{\nu}_\mu$ Beam Detector and $\nu_\mu$ $bar{\nu}_\mu$ Beam Source by Interaction between an Electron Bunch and a Positive Ion Bunch*; Mar. 1998

NIFS-545 J. Uramoto,
*Various Neutrino Beams Generated by $D_2$ Gas Discharge*; Mar.1998

NIFS-546 R Kanno, N. Nakajima, T Hayashi and M. Okamoto,
*Computational Study of Three Dimensional Equilibria with the Bootstrap Current*, Mar. 1998

NIFS-547 R. Kanno, N. Nakajima and M Okamoto,
*Electron Heat Transport in a Self-Similar Structure of Magnetic Islands*; Apr 1998

NIFS-548 J.E. Rice,
*Simulated Impurity Transport in LHD from MIST*; May 1998

NIFS-549 M.M. Skoric, T. Sato, A.M. Maluckov and M.S. Jovanovic,
*On Kinetic Complexity in a Three-Wave Interaction;* June 1998

NIFS-550 S. Goto and S. Kida,
*Passive Saclar Spectrum in Isotropic Turbulence: Prediction by the Lagrangian Direct-interaction Approximation;* June 1998

NIFS-551 T. Kuroda, H. Sugama, R. Kanno, M. Okamoto and W. Horton,
*Initial Value Problem of the Toroidal Ion Temperature Gradient Mode ;* June 1998

NIFS-552 T. Mutoh, R. Kumazawa, T. Seki, F. Simpo, G. Nomura, T. Ido and T. Watari,
*Steady State Tests of High Voltage Ceramic Feedthoughs and Co-Axial Transmission Line of ICRF Heating System for the Large Helical Device ;* June 1998

NIFS-553 N Noda, K. Tsuzuki, A. Sagara, N. Inoue, T. Muroga,
*oronaization in Future Devices -Protecting Layer against Tritium and Energetic Neutrals-:* July 1998

NIFS-554 S. Murakami and H. Saleem,
*Electromagnetic Effects on Rippling Instability and Tokamak Edge Fluctuations*; July 1998

NIFS-555 H. Nakamura , K. Ikeda and S. Yamaguchi ,
*Physical Model of Nernst Element*; Aug. 1998

NIFS-556 H. Okumura, S. Yamaguchi, H. Nakamura, K. Ikeda and K. Sawada,
*Numerical Computation of Thermoelectric and Thermomagnetic Effects*; Aug 1998

NIFS-557 Y. Takeiri, M Osakabe, K. Tsumori, Y. Oka, O. Kaneko, E. Asano, T. Kawamoto, R. Akiyama and M Tanaka,
*Development of a High-Current Hydrogen-Negative Ion Source for LHD-NBI System*; Aug.1998

NIFS-558 M. Tanaka, A. Yu Grosberg and T. Tanaka,
*Molecular Dynamics of Structure Organization of Polyampholytes*;Sep. 1998

NIFS-559 R. Horiuchi, K. Nishimura and T Watanabe,
*Kinetic Stabilization of Tilt Disruption in Field-Reversed Configurations*; Sep. 1998
(IAEA-CN-69/THP1/11)

NIFS-560 S. Sudo, K. Kholopenkov, K. Matsuoka, S. Okamura, C. Takahashi, R. Akiyama, A. Fujisawa, K. Ida, H. Idei, H. Iguchi, M. Isobe, S. Kado, K. Kondo, S. Kubo, H. Kuramoto, T. Minami, S. Morita, S. Nishimura, M. Osakabe, M. Sasao, B. Peterson, K. Tanaka, K. Toi and Y. Yoshimura,
*Particle Transport Study with Tracer-Encapsulated Solid Pellet Injection*;Oct 1998
(IAEA-CN-69/EXP1/18)

NIFS-561 A. Fujisawa, H. Iguchi, S. Lee, K. Tanaka, T. Minami, Y. Yoshimura, M. Osakabe, K. Matsuoka, S. Okamura, H. Idei, S. Kubo, S. Ohdachi, S. Morita, R. Akiyama, K. Toi, H. Sanuki, K. Itoh, K. Ida, A. Shimizu, S. Takagi, C. Takahashi, M. Kojima, S. Hidekuma, S. Nishimura, M. Isobe, A. Ejiri, N. Inoue, R. Sakamoto, Y. Hamada and M. Fujiwara,
*Dynamic Behavior Associated with Electric Field Transitions in CHS Heliotron/Torsatron*; Oct. 1998
(IAEA-CN-69/EX5/1)

NIFS-562 S. Yoshikawa,
*Next Generation Toroidal Devices*; Oct. 1998

NIFS-563 Y. Todo and T Sato,
*Kinetic-Magnetohydrodynamic Simulation Study of Fast Ions and Toroidal Alfvén Eigenmodes*; Oct. 1998
(IAEA-CN-69/THP2/22)

NIFS-564 T. Watari, T. Shimozuma, Y Takeiri, R Kumazawa, T. Mutoh, M. Sato, O. Kaneko, K. Ohkubo, S. Kubo, H. Idei, Y Oka, M. Osakabe, T. Seki, K. Tsumori, Y. Yoshimura, R. Akiyama, T. Kawamoto, S. Kobayashi, F. Shimpo, Y. Takita, E Asano, S. Itoh, G. Nomura, T. Ido, M. Hamabe, M. Fujiwara, A. Iiyoshi, S. Morimoto, T. Bigelow and Y.P. Zhao,
*Steady State Heating Technology Development for LHD*; Oct. 1998
(IAEA-CN-69/FTP/21)

NIFS-565 A. Sagara, K.Y. Watanabe, K. Yamazaki, O. Motojima, M. Fujiwara, O. Mitarai, S. Imagawa, H. Yamanishi, H. Chikaraishi, A. Kohyama, H. Matsui, T. Muroga, T. Noda, N. Ohyabu, T. Satow, A.A. Shishkin, S. Tanaka, T. Terai and T. Uda,
*LHD-Type Compact Helical Reactors*;Oct. 1998
(IAEA-CN-69/FTP/03(R)

NIFS-566 N Nakajima, J Chen, K Ichiguchi and M. Okamoto,
*Global Mode Analysis of Ideal MHD Modes in L=2 Heliotron/Torsatron Systems*, Oct 1998
(IAEA-CN-69/THP1/08)

NIFS-567 K Ida, M Osakabe, K Tanaka, T Minami, S Nishimura, S Okamura, A. Fujisawa, Y Yoshimura, S Kubo, R Akiyama, D S Darrow, H Idei, H Iguchi, M Isobe, S. Kado, T Kondo, S Lee, K Matsuoka, S Morita, I Nomura, S Ohdachi, M Sasao, A Shimizu, K Tumori, S Takayama, M Takechi, S Takagi, C Takahashi, K Toi and T Watari,
*Transition from L Mode to High Ion Temperature Mode in CHS Heliotron/Torsatron Plasmas*, Oct 1998
(IAEA-CN-69/EX2/2)

NIFS-568 S. Okamura, K. Matsuoka, R Akiyama, D S Darrow, A Ejiri, A Fujisawa, M Fujiwara, M Goto, K. Ida H Idei, H Iguchi, N Inoue, M Isobe, K Itoh, S Kado, K. Khlopenkov, T Kondo, S. Kubo, A Lazaros, S Lee, G Matsunaga, T Minami, S Morita, S Murakami, N Nakajima, N Nikai, S. Nishimura, I Nomura, S Ohdachi, K. Ohkuni, M Osakabe, R. Pavlichenko, B Peterson, R Sakamoto, H. Sanuki, M. Sasao, A. Shimizu, Y Shirai, S. Sudo, S Takagi, C. Takahashi, S Takayama, M Takechi, K Tanaka, K. Toi, K Yamazaki, Y Yoshimura and T Watari,
*Confinement Physics Study in a Small Low-Aspect-Ratio Helical Device CHS*, Oct 1998
(IAEA-CN-69/OV4/5)

NIFS-569 M.M. Skoric, T. Sato, A. Maluckov, M S Jovanovic,
*Micro- and Macro-scale Self-organization in a Dissipative Plasma*; Oct. 1998

NIFS-570 T. Hayashi, N Mizuguchi, T-H Watanabe, T Sato and the Complexity Simulation Group,
*Nonlinear Simulations of Internal Reconnection Event in Spherical Tokamak*; Oct 1998
(IAEA-CN-69/TH3/3)

NIFS-571 A. Iiyoshi, A Komori, A Ejiri, M. Emoto, H Funaba, M Goto, K Ida, H Idei, S Inagaki, S Kado, O Kaneko, K Kawahata, S Kubo, R. Kumazawa, S Masuzaki, T. Minami, J. Miyazawa, T. Morisaki, S. Morita, S Murakami, S Muto, T Muto, Y. Nagayama, Y Nakamura, H Nakanishi, K. Narihara, K Nishimura, N. Noda, T Kobuchi, S Ohdachi, N. Ohyabu, Y. Oka, M. Osakabe, T Ozaki, B.J. Peterson, A. Sagara, S. Sakakibara, R Sakamoto, H Sasao, M Sasao, K. Sato, M. Sato, T. Seki, T Shimozuma, M. Shoji, H Suzuki, Y. Takeiri, K. Tanaka, K Toi, T. Tokuzawa, K Tsumori, I Yamada, H. Yamada, S. Yamaguchi, M. Yokoyama, K.Y.Watanabe, T Watari, R Akiyama, H Chikaraishi, K Haba, S. Hamaguchi, S. Iima, S. Imagawa, N Inoue, K Iwamoto, S. Kitagawa, Y Kubota, J Kodaira, R Maekawa, T. Mito T. Nagasaka, A. Nishimura, Y Takita, C. Takahashi, K. Takahata, K. Yamauchi, H. Tamura, T Tsuzuki, S. Yamada, N Yanagi, H. Yonezu, Y. Hamada, K. Matsuoka, K. Murai, K. Ohkubo, I Ohtake, M Okamoto, S. Sato, T. Satow, S. Sudo, S. Tanahashi, K. Yamazaki, M. Fujiwara and O Motojima,
*An Overview of the Large Helical Device Project;* Oct 1998
(IAEA-CN-69/OV1/4)

NIFS-572 M. Fujiwara, H Yamada, A. Ejiri, M. Emoto, H Funaba, M. Goto, K Ida, H. Idei, S. Inagaki, S. Kado, O. Kaneko, K. Kawahata, A. Komori, S. Kubo, R Kumazawa, S Masuzaki, T. Minami, J Miyazawa, T Morisaki, S Morita, S. Murakami, S. Muto, T. Muto, Y Nagayama, Y. Nakamura, H. Nakanishi, K. Narihara, K. Nishimura, N. Noda, T. Kobuchi, S. Ohdachi, N. Ohyabu, Y. Oka, M. Osakabe, T. Ozaki, B. J. Peterson, A. Sagara, S. Sakakibara, R Sakamoto, H. Sasao, M. Sasao, K Sato, M Sato, T. Seki, T. Shimozuma, M. Shoji, H. Sazuki, Y Takeiri, K. Tanaka, K Toi, T Tokuzawa, K. Tsumori, I. Yamada, S Yamaguchi, M Yokoyama, K Y. Watanabe, T. Watari, R. Akiyama, H. Chikaraishi, K. Haba, S. Hamaguchi, M. Iima, S. Imagawa, N. Inoue, K. Iwamoto, S Kitagawa, Y. Kubota, J. Kodaira, R. Maekawa, T. Mito, T Nagasaka, A. Nishimura, Y. Takita, C. Takahashi, K. Takahata, K Yamauchi, H. Tamura, T. Tsuzuki, S Yamada, N. Yanagi, H. Yonezu, Y. Hamada, K. Matsuoka, K. Murai, K Ohkubo, I Ohtake, M. Okamoto, S. Sato, T. Satow, S Sudo, S Tanahashi, K Yamazaki, O Motojima and A. Iiyoshi,
*Plasma Confinement Studies in LHD;* Oct 1998
(IAEA-CN-69/EX2/3)

NIFS-573 O. Motojima, K. Akaishi, H. Chikaraishi, H. Funaba, S. Hamaguchi, S Imagawa, S. Inagaki, N. Inoue, A Iwamoto, S. Kitagawa, A Komori, Y. Kubota, R Maekawa, S. Masuzaki, T Mito, J Miyazawa, T. Morisaki, T Muroga, T Nagasaka, Y. Nakmura, A Nishimura, K. Nishimura, N. Noda, N. Ohyabu, S. Sagara, S. Sakakibara, R. Sakamoto, S. Satoh, T. Satow, M. Shoji, H. Suzuki, K Takahata, H Tamura, K. Watanabe, H Yamada, S. Yamada, S Yamaguchi, K. Yamazaki, N Yanagi, T Baba, H Hayashi, M. Iima, T. Inoue, S. Kato, T. Kato, T Kondo, S Monuchi, H. Ogawa, I. Ohtake, K Ooba, H. Sekiguchi, N. Suzuki, S. Takami, Y. Taniguchi, T Tsuzuki, N Yamamoto, K. Yasui, H Yonezu, M. Fujiwara and A. Iiyoshi,
*Progress Summary of LHD Engineering Design and Construction;* Oct 1998
(IAEA-CN-69/FT2/1)

NIFS-574 K. Toi, M. Takechi, S. Takagi, G. Matsunaga, M. Isobe, T. Kondo, M. Sasao, D S. Darrow, K. Ohkuni, S Ohdachi, R. Akiyama A Fujisawa, M. Gotoh, H Idei, K Ida, H. Iguchi, S Kado, M Kojima, S. Kubo, S. Lee, K. Matsuoka, T Minami, S. Morita, N Nikai, S Nishimura, S Okamura, M Osakabe, A. Shimizu, Y Shirai, C. Takahashi, K. Tanaka, T Watari and Y. Yoshimura,
*Global MHD Modes Excited by Energetic Ions in Heliotron/Torsatron Plasmas*; Oct. 1998
(IAEA-CN-69/EXP1/19)

NIFS-575 Y. Hamada, A. Nishizawa, Y Kawasumi, A. Fujisawa, M. Kojima, K. Narihara, K Ida, A. Ejiri, S. Ohdachi, K. Kawahata, K Toi, K. Sato, T. Seki, H Iguchi, K Adachi, S Hidekuma, S.Hirokura, K. Iwasaki, T. Ido, R. Kumazawa, H. Kuramoto, T Minami, I Nomura, M. Sasao, K N. Sato, T. Tsuzuki, I Yamada and T. Watari,
*Potential Turbulence in Tokamak Plasmas*, Oct. 1998
(IAEA-CN-69/EXP2/14)

NIFS-576 S. Murakami, U. Gasparino, H. Idei, S. Kubo, H Maassberg, N Marushchenko, N Nakajima, M. Romé and M. Okamoto,
*5D Simulation Study of Suprathermal Electron Transport in Non-Axisymmetric Plasmas*; Oct 1998
(IAEA-CN-69/THP1/01)

NIFS-577 S. Fujiwara and T Sato,
*Molecular Dynamics Simulation of Structure Formation of Short Chain Molecules*; Nov 1998

NIFS-578 T. Yamagishi,
*Eigenfunctions for Vlasov Equation in Multi-species Plasmas* Nov. 1998

NIFS-579 M. Tanaka, A. Yu Grosberg and T. Tanaka,
*Molecular Dynamics of Strongly-Coupled Multichain Coulomb Polymers in Pure and Salt Aqueous Solutions*;Nov. 1998

NIFS-580 J. Chen, N. Nakajima and M. Okamoto,
*Global Mode Analysis of Ideal MHD Modes in a Heliotron/Torsatron System: I. Mercier-unstable Equilibria*;Dec. 1998

NIFS-581 M Tanaka, A. Yu Grosberg and T. Tanaka,
*Comparison of Multichain Coulomb Polymers in Isolated and Periodic Systems: Molecular Dynamics Study;* Jan 1999

NIFS-582 V.S. Chan and S. Murakami,
*Self-Consistent Electric Field Effect on Electron Transport of ECH Plasmas*; Feb. 1999

NIFS-583 M. Yokoyama, N. Nakajima, M. Okamoto, Y. Nakamura and M. Wakatani,
*Roles of Bumpy Field on Collisionless Particle Confinement in Helical-Axis Heliotrons*;Feb. 1999

NIFS-584 T.-H. Watanabe, T. Hayashi, T. Sato, M. Yamada and H. Ji,
*Modeling of Magnetic Island Formation in Magnetic Reconnection Experiment*,Feb 1999

NIFS-585 R. Kumazawa, T. Mutoh, T. Seki, F. Shinpo, G. Nomura, T Ido, T. Watari, Jean-Marie Noterdaeme and Yangping Zhao,
*Liquid Stub Tuner for Ion Cyclotron Heating*;Mar. 1999

NIFS-586 A. Sagara, M. Iima, S. Inagaki, N. Inoue, H. Suzuki, K. Tsuzuki, S. Masuzaki, J. Miyazawa, S. Morita, Y Nakamura, N. Noda, B. Peterson, S. Sakakibara, T. Shimozuma, H Yamada, K. Akaishi, H. Chikaraishi, H. Funaba, O. Kaneko, K. Kawahata, A. Komori, N. Ohyabu, O. Motojima, LHD Exp. Group 1, LHD Exp Group 2,
*Wall Conditioning at the Starting Phase of LHD*;Mar. 1999

NIFS-587 T. Nakamura and T. Yabe,
*Cubic Interpolated Propagation Scheme for Solving the Hyper-Dimensional Vlasov-Poisson Equation in Phase Space*;Mar. 1999

NIFS-588 W.X. Wnag, N. Nakajima, S. Murakami and M. Okamoto,
*An Accurate $\delta f$ Method for Neoclassical Transport Calculation* ;Mar. 1999

NIFS-589 K. Kishida, K. Araki, S. Kishiba and K. Suzuki,
*Local or Nonlocal? Orthonormal Divergence-free Wavelet Analysis of Nonlinear Interactions in Turbulence*;Mar. 1999

NIFS-590 K. Araki, K. Suzuki, K. Kishida and S. Kishiba,
*Multiresolution Approximation of the Vector Fields on $T^3$*;Mar. 1999

NIFS-591 K. Yamazaki, H. Yamada, K.Y.Watanabe, K. Nishimura, S. Yamaguchi, H Nakanishi, A. Komori, H. Suzuki, T Mito, H. Chikaraishi, K. Murai, O. Motojima and the LHD Group,
*Overview of the Large Helical Device (LHD) Control System and Its First Operation*,Apr. 1999

NIFS-592 T. Takahashi and Y. Nakao,
*Thermonuclear Reactivity of D-T Fusion Plasma with Spin-Polarized Fuel*; Apr 1999

NIFS-593 H. Sugama,
*Damping of Toroidal Ion Temperature Gradient Modes*; Apr. 1999

NIFS-594 Xiaodong Li ,
*Analysis of Crowbar Action of High Voltage DC Power Supply in the LHD ICRF System*; Apr. 1999

NIFS-595 K. Nishimura, R. Horiuchi and T. Sato,
*Drift-kink Instability Induced by Beam Ions in Field-reversed Configurations*; Apr. 1999